

# ***In situ* measurement of annealing-induced line shape evolution in nanoimprinted polymers using scatterometry**

Heather J. Patrick,<sup>1,2,\*</sup> Thomas A. Germer,<sup>1</sup> Yifu Ding,<sup>3</sup>  
Hyun Wook Ro,<sup>1</sup> Lee J. Richter,<sup>1</sup> and Christopher L. Soles<sup>1</sup>

<sup>1</sup>*National Institute of Standards and Technology, Gaithersburg, MD 20899 USA*

<sup>2</sup>*KT Consulting, Inc., Antioch, CA 94509 USA*

<sup>3</sup>*Department of Mechanical Engineering, University of Colorado, Boulder, CO 80309 USA*

## **ABSTRACT**

Thermal embossing nanoimprint lithography (NIL) is an area of continuing interest because it allows direct patterning of nanoscale structures into a wide variety of functional polymer materials. Measuring the shape evolution of nanoimprinted lines during thermal annealing can provide insights into mechanisms of polymer stability and the dynamics of polymer flow. Recently, we have used optical scatterometry to extract the profile of nanoimprinted lines in low- and high-molecular mass polymer gratings during annealing of the gratings at the glass transition temperature. The data are obtained *in situ* using a spectroscopic ellipsometer and analyzed using a rigorous-coupled-wave scatterometry model. The results obtained from scatterometry are in very good agreement with those measured *ex situ* by atomic force microscopy and specular x-ray reflectivity, revealing very different decay mechanisms for gratings in low- and high-molecular mass polymers. The role of the selection of grating model in determining the uncertainties the grating line profile extracted from scatterometry is also discussed.

**Keywords:** nanoimprint, optical critical dimension, polymers, scatterometry, spectroscopic ellipsometry, stress, rheology

## **1. INTRODUCTION**

Nanoimprint lithography (NIL), in which features on a pre-patterned mold are transferred directly into a polymer material, is a rapidly maturing alternative to optical techniques for nanoscale patterning of semiconductors. One method, thermal embossing NIL, can also be used to directly pattern functional polymers, e.g., those that have semiconducting, piezoelectric, or insulating properties. Understanding the stability and decay mechanisms of these as-imprinted structures is crucial to the development of thermal embossing NIL. Prior studies have shown that measuring the shape evolution (reflow) of nanoimprinted lines during thermal annealing can provide important information about the stability of patterns of different molecular masses, the expected impact of mold release temperature on pattern shapes, and the roles of residual stresses and polymer viscosity on pattern stability.<sup>1,2,3,4</sup>

Recently, we have been investigating the use of scatterometry to provide *in situ*, non-destructive measurements of line gratings in nanoimprinted polymers during annealing.<sup>5</sup> In contrast with pattern characterization through cross-section scanning electron microscopy (SEM) or atomic force microscopy (AFM), which are time consuming, require sectioning of the sample (in the case of SEM), and typically require multiple samples annealed for different times to build up a complete picture of the annealing response, scatterometry provides a real-time annealing record from a single sample and, with appropriate model development, can be used to extract line shape parameters at any point during the anneal. We will review recent results from scatterometry analysis of gratings measured *in situ* by spectroscopic ellipsometry during annealing and show that line parameters obtained from scatterometry are in very good agreement with values obtained using AFM and specular x-ray reflectivity (SXR). Finally, we present results obtained by using three different scatterometry line profile models to analyze a subset of the spectroscopic ellipsometry data, as part of an effort to quantify uncertainties in the line profiles obtained from scatterometry.

\*Correspondence: heather.patrick@nist.gov

## 2. EXPERIMENT

The nanoimprinted gratings were prepared from thin films of polystyrene (PS) with molar masses of  $18.1 \text{ kg mol}^{-1}$  and  $1571 \text{ kg mol}^{-1}$ , referred to here as PS18k and PS1570k. Samples of the PS in toluene solution were spin coated onto Si wafers, then annealed in vacuum at  $150 \text{ }^\circ\text{C}$  for 1 h to remove the solvent. The resulting  $\sim 300 \text{ nm}$  thick films were imprinted on a Nanonex NX-2000 imprinter,<sup>6</sup> using a silicon oxide imprinting mold that had multiple line and space gratings of  $420 \text{ nm}$  pitch, height of  $\sim 360 \text{ nm}$ , and a line to space ratio of 1:1.6. The area of each grating was  $5 \text{ mm} \times 20 \text{ mm}$ . The mold was coated with a fluorinated self-assembled monolayer to facilitate release after imprinting. The PS films were imprinted under vacuum at a temperature  $40 \text{ }^\circ\text{C}$  above the glass transition temperature ( $T_g$ ) of the bulk polymer, then cooled to  $55 \text{ }^\circ\text{C}$  before release from the mold. The imprinted wafer was divided into individual  $5 \text{ mm} \times 20 \text{ mm}$  or  $5 \text{ mm} \times 10 \text{ mm}$  grating chips to provide samples for the annealing experiments. Additional details of the imprinting procedure can be found in Ref. 1.

We used spectroscopic ellipsometry (SE) to characterize the imprinted gratings and the as-spun PS films. The ellipsometric parameters<sup>7</sup>  $\alpha$  and  $\beta$  were measured at 616 points over a wavelength range of  $335 \text{ nm}$  to  $1700 \text{ nm}$  using a Woollam M-2000 rotating compensator variable-angle spectroscopic ellipsometer. Although the ellipsometer's wavelength range extends to  $190 \text{ nm}$  with an ultraviolet (uv) lamp, the uv lamp was turned off for the current study because it visibly damaged gratings in preliminary measurements. The size of the measurement spot on the sample was approximately  $0.3 \text{ mm}$  wide and  $0.4 \text{ mm}$  to  $1.2 \text{ mm}$  long, depending upon the incident angle. For gratings, the incident angle was fixed at  $60^\circ$  from normal, and the grating chip was aligned with the grating lines perpendicular to the plane of incidence. When measuring a film, SE spectra were taken at  $45^\circ$ ,  $60^\circ$ , and  $75^\circ$ .

To anneal the gratings, a calibrated hot stage was mounted on the ellipsometer sample stage. To perform an annealing run, a grating chip was initially aligned on the ellipsometer at room temperature and then removed from the stage. The stage was then preheated to the  $T_g$  of the PS (either  $100 \text{ }^\circ\text{C}$  for PS18k, or  $106 \text{ }^\circ\text{C}$  for PS1570k), and the chip was replaced on the preheated stage. We estimate the accuracy of the temperature set point to be  $\pm 1 \text{ }^\circ\text{C}$ , obtained from the use of a benzil melting point standard. Ellipsometry data acquisition was begun following a  $1.5 \text{ min}$  delay in order to verify chip alignment. Ellipsometric spectra were then acquired every  $12 \text{ s}$  over the next two hours. Figs. 1(a) and 1(b) show ellipsometric spectra for the PS18k grating at three times during annealing. In addition to the *in situ* annealing, a number of chips were annealed on the stage at fixed temperature for times ranging from  $3 \text{ min}$  to  $180 \text{ min}$ , in order to obtain a set of samples with a range of pattern decay conditions for later comparison *ex situ* using SE, SXR and AFM.

## 3. MODELING

The grating ellipsometry spectra were fit to a rigorous-coupled-wave (RCW) scatterometry model. In scatterometry, we develop a parameterized model for the shape of the lines in a grating using *a priori* knowledge of the line structure and then calculate theoretical ellipsometric spectra for different combinations of the line parameters.<sup>8</sup> The model assumes the grating consists of a periodic array of lines. The combination of parameters giving the best fit to the measured data is determined by library matching or regression analysis. The model is necessarily an approximation to the true grating structure, so it is important to note that it cannot identify features outside of the parameter space provided to the model. The validity of a model is generally determined by evaluating the quality of the fit it gives to the experimental data and by the correlation of the scatterometry results to those obtained by other techniques.

In our initial investigations, we have employed a scatterometry model that includes a residual PS layer and grating lines that can vary in cross section from a slightly smoothed trapezoid to nearly sinusoidal by increasing the amount of edge smoothing. We obtain this profile by numerically convolving a trapezoid with a Gaussian. Some line profiles from this model, which will be referred to as the Gaussian-convolved trapezoid (GCT) model, are shown in Fig. 1(c). Alternative models will be discussed in Section 6. Theoretical ellipsometric signatures were obtained using the RCW analysis for surface relief gratings.<sup>9,10,11</sup> This method solves the electromagnetic problem for a plane wave incident upon a one-dimensionally periodic grating. The vertical profile of the grating is divided into 20 layers in order to capture the corner rounding of the gratings. In practice, the Floquet expansions of the fields are truncated at some maximum order

$M$ ; for these samples  $M$  was chosen to be 5, which was found to be sufficient for these polymer structures. The code implemented by NIST for generating theoretical signatures is publicly available.<sup>12</sup>

The GCT model was parameterized by top and bottom widths and the height of the trapezoid, residual layer thickness, pitch, and the width of the Gaussian. The pitch of the gratings was fixed at 419.8 nm as measured by laser diffractometry. The silicon substrate dispersion (i.e., the optical constants  $n$  and  $k$  as a function of wavelength  $\lambda$ ) was taken from the literature<sup>13</sup> and was held fixed in the model. The dispersion curves for PS18k and PS1570k were measured from ellipsometry of thin films of the materials; separate dispersion curves were produced from hot (at  $T_g$ ) and room temperature films and used appropriately.

Fitting of the ellipsometry data to the model was done by minimizing the figure of merit  $\chi_r^2$ , given by

$$\chi_r^2 = \frac{1}{(2N - \nu)} \sum_{j=1}^N \left[ \left( \frac{\alpha(\lambda_j) - \alpha_{\text{theory}}(\lambda_j)}{\sigma_\alpha(\lambda_j)} \right)^2 + \left( \frac{\beta(\lambda_j) - \beta_{\text{theory}}(\lambda_j)}{\sigma_\beta(\lambda_j)} \right)^2 \right] \quad (1)$$

where  $N = 617$  is the number of discrete wavelengths  $\lambda_j$  where the ellipsometric parameters  $\alpha$  and  $\beta$  were measured,  $\nu$  is the number of line parameters varied when generating the theoretical  $\alpha_{\text{theory}}$  and  $\beta_{\text{theory}}$  signatures, and  $\sigma_\alpha(\lambda_j)$  and  $\sigma_\beta(\lambda_j)$  are estimated uncertainties in the measured  $\alpha$  and  $\beta$ . This equation is the familiar reduced- $\chi^2$ ,<sup>14</sup> which is used as a relative measure of goodness-of-fit for different parameter sets. The parameter set with the smallest  $\chi_r^2$  gives the best estimate of the line parameters for the sample, within the limits of the theoretical line profile model that was chosen. For the annealing experiments, initial fits to the as-imprinted grating samples were made using a library of trapezoidal profiles with minimal smoothing; after the best fit profile was found, the data taken during subsequent spectra were fit by Levenberg-Marquardt regression using the parameters from the previous spectra as initial conditions. In this way a full time record of the line profile evolution during annealing was built up. A similar fitting procedure was used for the series of *ex situ* samples: within a given polymer type, spectra were fit in order of annealing time, starting with the shortest.

#### 4. IN SITU ANNEALING RESULTS

Figure 1 shows typical ellipsometry  $\alpha$  and  $\beta$  spectra (solid lines) at three times during annealing of a PS18k grating at  $T_g = 100$  °C. The best fits to the data, obtained using the GCT profile described above, are also shown (dashed lines). Looking at the spectra, we can see characteristic features of the residual layer and grating modulation as they change during annealing. For example, in the  $\alpha$  spectra, the broad peaks around 600 nm and 1500 nm are associated in part with the residual layer thickness. Sharper features like the peaks around 480 nm and 800 nm are associated with the grating modulation, which decreases with annealing time. In Fig. 1(c), the GCT line profiles corresponding to the fits in Figs. 1(a) and 1(b) are shown, with the total height of the PS from the Si substrate surface on the y axis. An advantage of scatterometry profiling, in addition to its speed, is that—as with SXR, but unlike AFM—the residual layer thickness can be extracted along with the grating line profiles.

For the fits shown in Figs. 1(a) and 1(b),  $\chi_r^2$  ranged from 75 (for 31.7 min) to 287 (for 1.7 min). For data with statistically distributed noise, a “good fit” is generally expected to have  $\chi_r^2 \approx 1$ .<sup>14</sup> However, as is typical in scatterometry and ellipsometry,  $\chi_r^2$  is dominated by systematic deviations in some parts of the fit, because the model is never a perfect representation of the grating structure and the presence of systematic errors in the data.<sup>8,15</sup> The presence of significant systematic deviations between data and theory make an objective determination of goodness of fit, and thus a statistically meaningful determination of the uncertainty in the extracted parameters, difficult.<sup>14,16</sup>  $\chi_r^2$  is primarily used to evaluate the relative quality of fits for different parameter combinations in the model, and to compare the results of different grating models. Different grating models will be discussed further in Section 6.

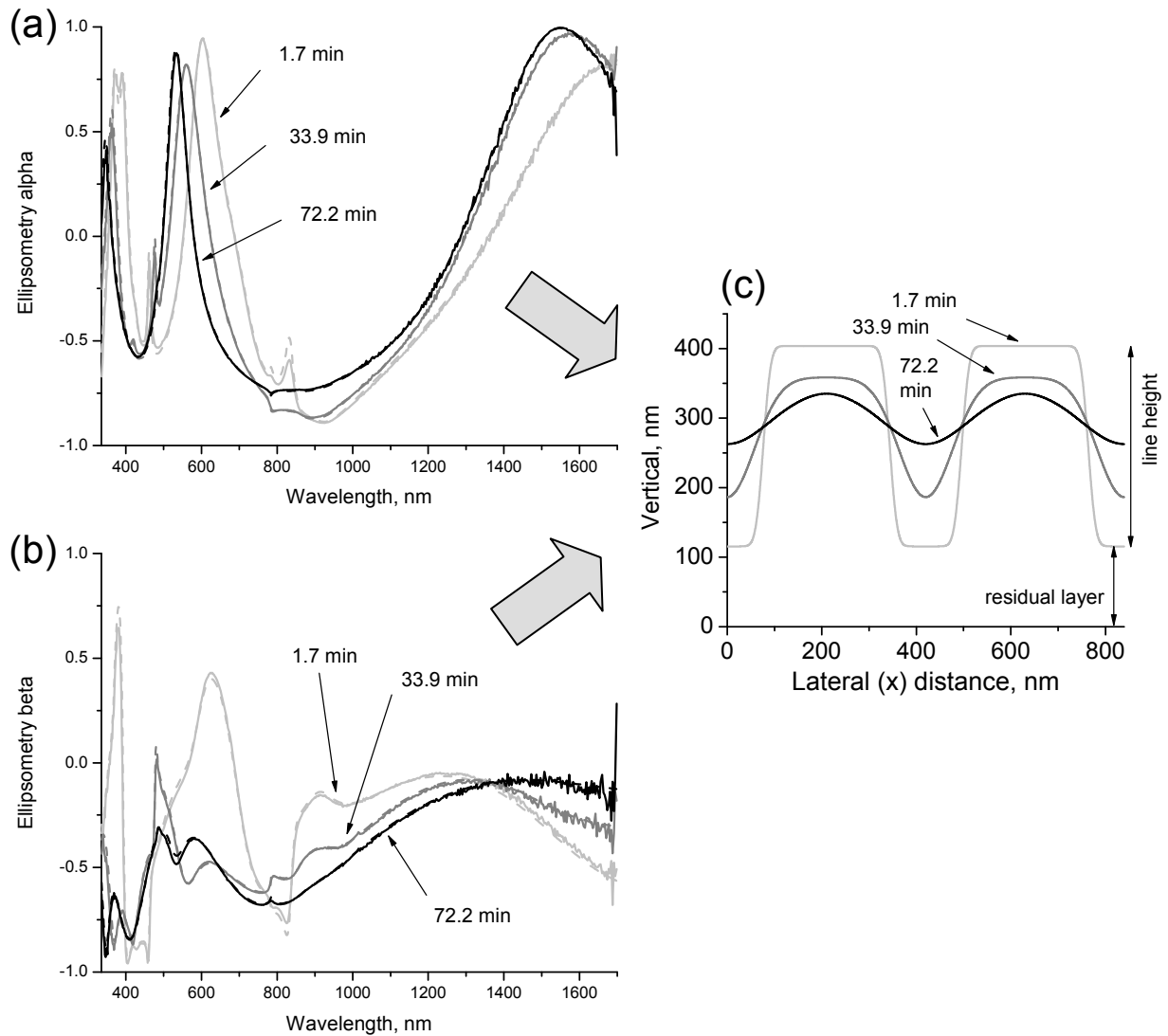


**FIG. 1** Ellipsometry (a)  $\alpha$  and (b)  $\beta$  measured during annealing of the PS18k grating at  $T_g = 100^\circ\text{C}$  and model fits to the data. In (a) and (b), data (solid lines) and scatterometry model fits (dashed lines) are shown at 1.7 min (light grey lines), 33.9 min (dark grey lines) and 72.8 min (black lines) into the anneal. The corresponding best fit line profiles are shown in (c), with the line height and residual layer thickness illustrated for the 1.7 min profile.

The evolution of grating height during reflow has been shown to provide crucial insight into polymer rheology,<sup>1,2,3</sup> and the *in situ* measurement used here provides a nearly continuous annealing record that can be used to obtain the grating height versus time. Figure 2 shows the line height extracted from the GCT scatterometry model versus time, for low molecular mass PS18k gratings and high molecular mass PS1570k gratings. The results indicate very different reflow kinetics for the two polymers. For a simple liquid with surface-tension-dominated viscous flow, the pattern height is expected to decay exponentially with time.<sup>1</sup> As seen in Fig. 2, the PS18k pattern decay is roughly consistent with this model, while the PS1570k pattern height shows a fast early relaxation that has been attributed to elastic recovery of residual stress locked into the more highly entangled, longer chain polymers during imprinting, followed by a plateau with a much slower decay rate. The measured height decay is consistent with results obtained by AFM in an earlier study.<sup>1</sup> Because the scatterometry results are obtained from a single chip *in situ*, a much higher density of sampling is feasible than with *ex situ* measurements.

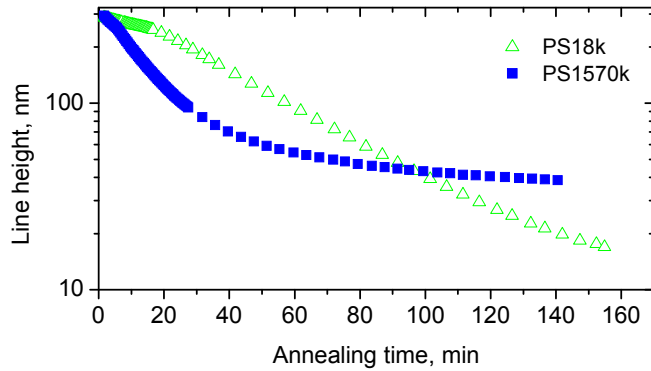


**FIG. 2.** Line height measured by scatterometry versus time, for a PS18k grating (open green triangles) during annealing at  $T_g = 100$  °C, and a PS1570k grating (closed blue squares) during annealing at  $T_g = 106$  °C.

As a first test for the validity of the measurement, we evaluated the volume conservation of the patterns. We obtain a full pattern profile at each time during the annealing, including grating and residual layer, allowing us to evaluate the total volume of the pattern at each time. This volume should remain constant during anneal. Figure 3 shows the extracted change in total volume of polymer associated with the GCT line profile for every point shown in Fig. 2, referenced to the volume in the first measured line profile. For both PS18k and PS1570k gratings, the volume conservation was better than 0.7 % peak-to-peak. Nearly all of the volume variation was observed early in the anneal, when we also obtained somewhat poorer fits to the profile model. The volumes obtained with other profile models, described later, showed similar variation in total volume. The results of this test, while appearing very good, does not so much validate the specific profile model used than demonstrate that the technique is very sensitive to the overall volume of the grating.

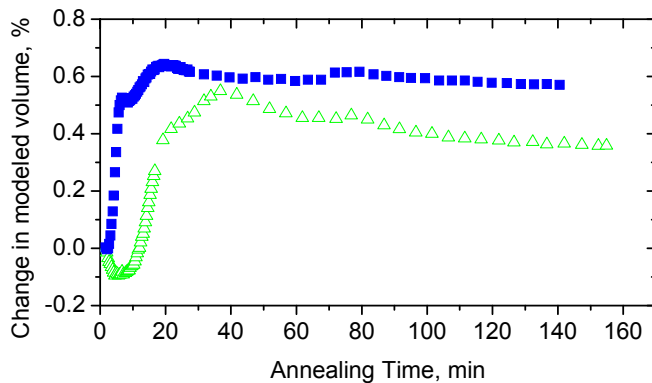


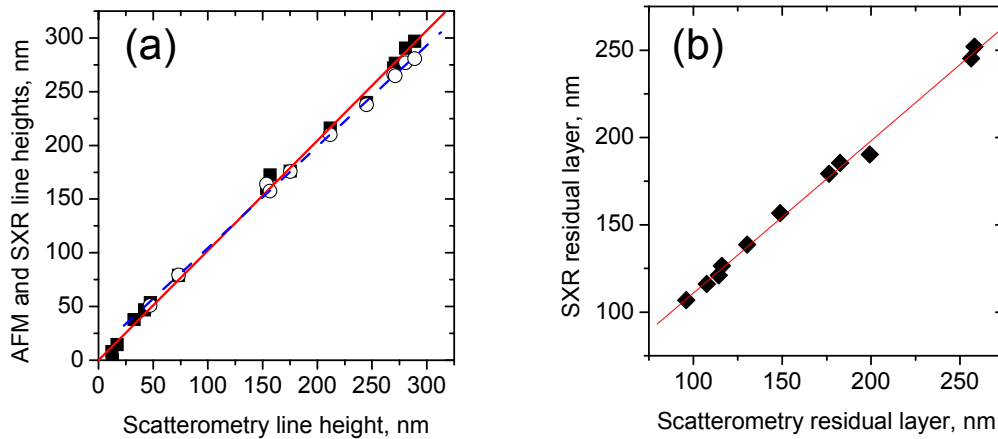
**FIG. 3.** Relative volume change measured by scatterometry (using the GCT profile) versus time, for a PS18k grating (open green triangles) during annealing at  $T_g = 100$  °C, and a PS1570k grating (closed blue squares) during annealing at  $T_g = 106$  °C.

## 5. COMPARISON OF SCATTEROMETRY TO AFM AND SXR

In this section, we compare the results of the GCT scatterometry line profiles with results obtained by AFM and SXR, for the set of *ex situ* samples with a range of pattern decay conditions. The AFM used here was restricted to mea-

measuring grating height; the size and shape of the AFM tip did not allow for more detailed line shape characterization.<sup>1</sup> SXR is an x-ray based technique that has recently been used to characterize pattern shapes of nanoimprint gratings.<sup>17</sup> For SXR, the specular reflected x-ray intensity signature of each grating sample was fit to a multi-layer model of material density versus depth. The residual layer thicknesses and line heights of the samples were extracted from the layer thicknesses. For a subset of the samples, the line shape was also extracted by converting the density of each layer to a line-space ratio on that layer using the grating pitch measured from laser diffractometry. The SXR method is described more fully in Ref. 17.

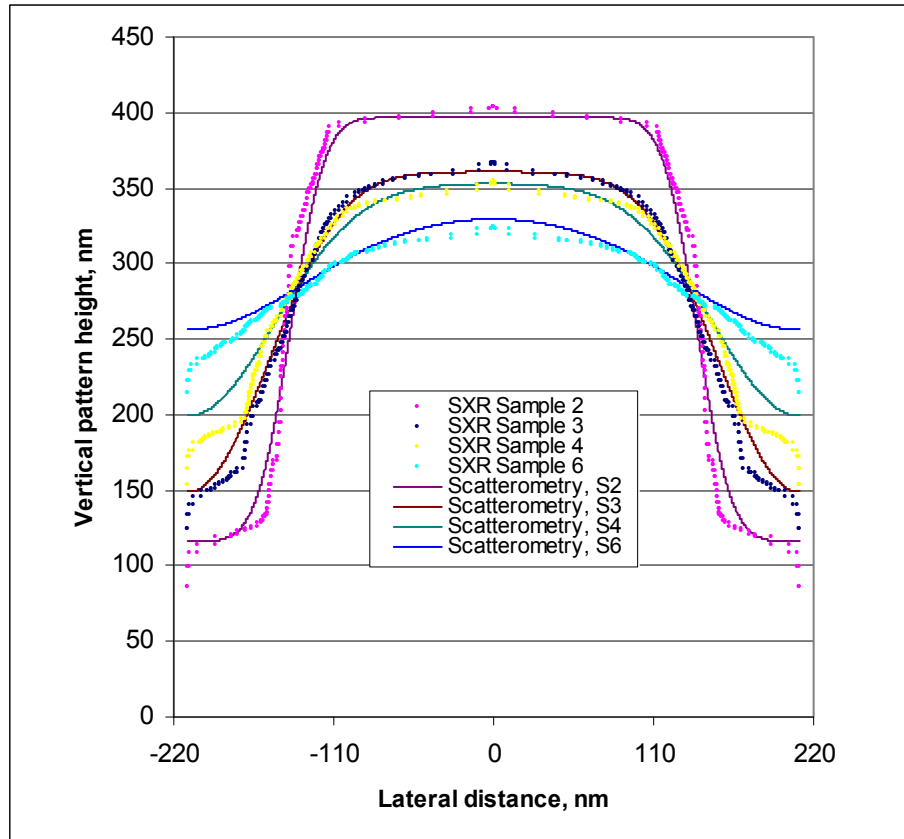
We first compare results for line height and residual layer thickness measured by scatterometry, AFM, and SXR. Figure 4(a) shows the comparison of line height measured by SXR and by AFM with line height measured by scatterometry using the GCT model. The agreement of scatterometry with the two techniques is excellent. While we have not carried out a full uncertainty analysis for each of the three techniques, an unweighted linear regression of AFM line height to scatterometry line height yielded a slope of  $1.02 \pm 0.02$  and an intercept of  $0.2 \text{ nm} \pm 2.7 \text{ nm}$ , and the linear fit of SXR line height to scatterometry line height yielded a slope of  $0.94 \pm 0.01$  and an intercept of  $10.3 \text{ nm} \pm 2.9 \text{ nm}$ .<sup>18</sup> In the case of SXR, samples with line heights less than about 50 nm did not give sufficient reflectance for successful SXR modeling, so these samples were not included. The residual layer values as measured by SXR and scatterometry, shown in Fig. 4(b), are also in fairly good agreement. An unweighted, linear fit of residual layer thickness measured by SXR to that measured by scatterometry yielded a slope of  $0.87 \pm 0.02$  and an intercept of  $23.6 \text{ nm} \pm 3.1 \text{ nm}$ . Sources of the difference between the two techniques are under investigation. Because SXR models the density of material versus depth, it can be difficult to exactly pinpoint the location of the transition between the bulk material and the grating, particularly for highly annealed samples with very rounded grating profiles. In the scatterometry case, the volume conservation observed for annealed gratings suggests that the residual layer thicknesses should be accurate, but this finding also depends on having an accurate profile for the grating modulation. We will discuss alternate profile models further in Section 6. An advantage of both techniques is that they can measure the residual layer thickness non-destructively.



**FIG. 4.** Comparison of scatterometry line parameters to those measured by AFM and SXR, for a series of *ex situ* measurements on annealed grating samples. (a) Line height measured by AFM (solid squares) and SXR (open circles) versus line height measured by scatterometry. Linear fits to the data, shown by the red solid line (AFM), and blue dashed line (SXR) are discussed in the text. (b) Thickness of the residual PS layer measured by SXR versus scatterometry. A straight line fit to the data is shown by the red solid line and is discussed in the text.

Figure 5 shows the cross-section profiles for a single period of four of the *ex situ* samples with a range of grating heights, with the gratings having smaller modulations corresponding to longer annealing times. The solid line profiles were obtained from scatterometry using the GCT model, while the profiles shown by individual points were generated using a multi-layer density profile model in SXR. This comparison is preliminary; we have attempted to match the scatterometry and SXR models near the tops of the lines, and there is significant SXR profile uncertainty at the edges of the line (i.e., the interface between solid film and the start of the grating trench). However, we see reasonable agreement

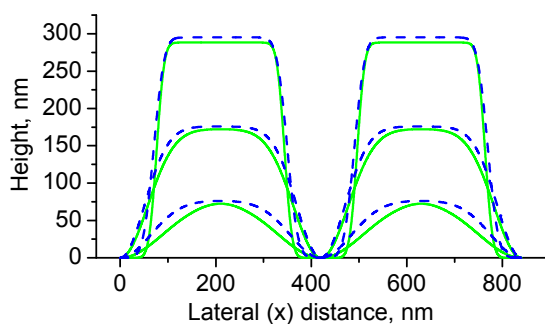
between SXR and scatterometry for the line shape well away from the trenches, with scatterometry and SXR profiles showing an increasingly rounded grating profile with increased annealing time.



**FIG. 5.** Comparison of line profile obtained using SXR modeling (curves with individual symbols) to those obtained from the GCT scatterometry model (solid line curves) for four PS18k gratings annealed for various times and measured *ex situ*.

## 6. SCATTEROMETRY PROFILE ANALYSIS

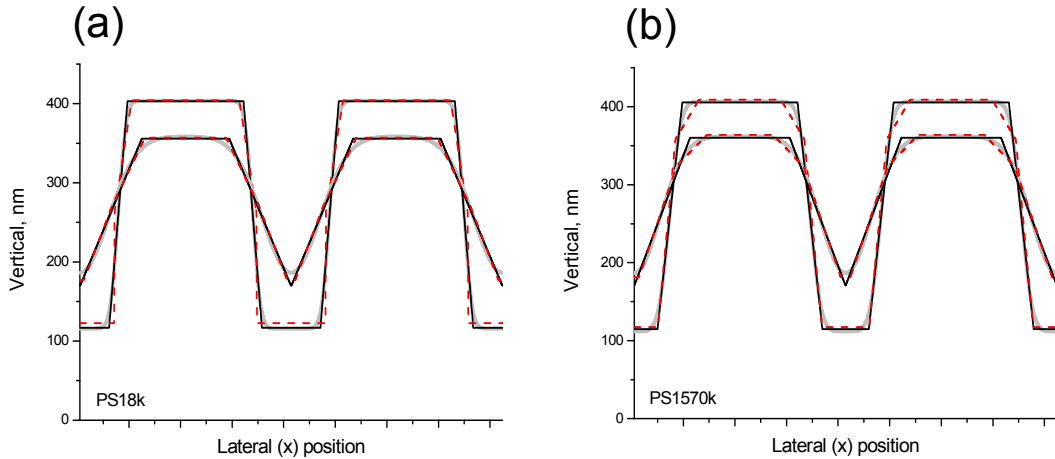
We now turn to the implications of the extracted GCT line profiles to models of polymer stability and to some exploratory efforts to address the role of the selection of line profile model in determining scatterometry uncertainties. We initially focus on the GCT grating profiles of the low and high molecular mass polymers at similar grating height, which has been discussed in more detail in Ref. 5. Figure 6 shows the GCT line profiles for the two polymers at the first point measured during annealing, then at  $\sim 175$  nm and  $\sim 75$  nm heights. It should be noted that because of the very different height decay rates (see Fig. 2), similar heights are obtained at different times during annealing of the two polymer mass gratings. While the profiles are initially similar, by 75 nm height, the PS18k grating profile is consistent with a sinusoid with 1:1 line to space ratio, while the PS1570k profile retains a broader line shape. The broader line shape of the PS1570k profile, along with deviation from simple exponential height decay seen in Fig. 2, is consistent with the hypothesis of Ref. 1 that elastic recovery, rather than viscous flow, dominates the high-molecular mass polymer decay. As a check on the low and high molecular mass profile differences, we also attempted to fit the ellipsometry spectra from both the PS18k and PS1570k gratings at 75 nm height using a sinusoidal line shape model. In the PS18k case, the fit of the ellipsometry data to the sinusoidal model had similar  $\chi_r^2$  to that given by the GCT profile, while for the PS1570k data, the  $\chi_r^2$  for the sinusoidal model was almost twice that for the broader line profile model shown in Fig. 6.



**FIG. 6.** Line profiles of the PS18k grating (green solid curves) and the PS1570k grating (blue dashed curves) for three similar grating heights. Note that the underlying residual PS layer is not shown.

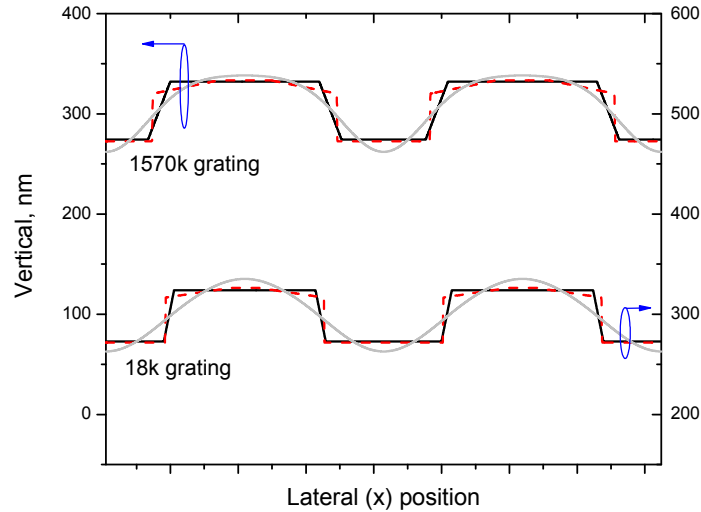
The problem of assigning independent uncertainties to the parameters obtained from scatterometry, and to the line profiles shown in Fig. 6, is complex. Because the raw ellipsometry data deviate systematically from the model in some parts of the spectra (see Fig. 1), as is typical in scatterometry measurements, we cannot perform a traditional  $\chi^2$  analysis<sup>14</sup> to determine the error in the extracted line profiles and parameters. In earlier work, we have used simulated data sets with true random noise added to approximate noise on an experimentally measured signal, in order to evaluate the relative confidence levels of different grating parameters, and to identify correlations between different parameters that can make independent measurements of these parameters challenging.<sup>16</sup> Work on extending scatterometry error analysis to account for systematic errors is ongoing.<sup>19</sup> Another important aspect of scatterometry modeling, however, is the restrictions imposed by the assumed line profile model on the extracted parameters. While the GCT model fits the ellipsometry data well and gives good agreement with other techniques for height and residual layer thickness, it is not the only profile that could be used to fit the data. To provide insight into the capabilities and limitations of the current GCT model, we also fit the ellipsometry spectra corresponding to the line profiles shown in Fig. 6 using two simpler models: a single trapezoid on a residual layer, and a double trapezoid on a residual layer. Neither trapezoidal profile included any corner rounding or smoothing. The single trapezoid line profile was parameterized by top and bottom linewidths, line height, residual layer thickness, and pitch. The double trapezoid line profile consisted of two stacked trapezoids, where the bottom linewidth of the upper trapezoid in the stack equals the top linewidth of the lower trapezoid, and the heights of the upper and lower trapezoid can vary independently. It was parameterized by top linewidth, the shared linewidth of the upper and lower trapezoids, the bottom linewidth, the total line height, a breakpoint between the trapezoids (expressed as a fraction of the total line height), the residual layer thickness, and the pitch. As in the original GCT simulations the pitch of the gratings was fixed at 419.8 nm and the material optical properties were fixed. The other parameters were allowed to vary during Levenberg-Marquardt regression to find the profile that minimized  $\chi_r^2$ .

Figure 7 shows the best fit line profiles given by the GCT, single trapezoid, and double trapezoid models for the *in situ* annealing data from the low- and high-molecular mass polymers at the first point during annealing and at  $\sim 175$  nm heights. The best fit single and double trapezoid profiles are in fairly good agreement with the GCT profiles, although the cutting off of the top corners, seen most clearly in the PS1570k profiles, suggests that the GCT model might be improved by incorporating independent rounding of the top and bottom corners of the line. (The current GCT model requires equal smoothing at the top and bottom corners, and assumes a basically single trapezoidal line profile.) In fact, a comparison of  $\chi_r^2$  obtained by fits to different line profile models suggests that early in the annealing, when the grating is expected to retain more of its as-imprinted shape, the inclusion of multiple trapezoids may be more important than incorporating corner rounding. While the fits that correspond to the single line trapezoid profiles shown in Fig. 7 all have larger  $\chi_r^2$  than those to the GCT profile, the double trapezoid profiles resulted in a smaller  $\chi_r^2$  than obtained by the GCT model, particularly for the PS1570k grating. The interpretation of this surprising result is not completely clear; it should be remembered that the  $\chi_r^2$  in all cases is much larger than 1 and is dominated by systematic deviations in a few regions of the spectra. The fits for all the profile models appear by the eye to be quite good, similar to the fits using the GCT model shown in Fig. 1, but because the differences between fit and data are dominated by systematic deviations in a few regions in the spectra, trade-offs between fit quality in different spectral regions can result in lower total  $\chi_r^2$ .



**FIG. 7.** Comparison of best fit line profiles obtained using three line profile models. In (a) line profiles for the PS18k grating at initial height and  $\sim 175$  nm height are shown using the GCT model (light grey solid lines) the single trapezoid model (solid black lines) and the double trapezoid model (dashed red lines). In (b) line profiles for the PS1570k grating at initial height and  $\sim 175$  nm height are shown using the GCT model (light grey solid lines) the single trapezoid model (solid black lines) and the double trapezoid model (dashed red lines).

For spectra taken later in the annealing, when the gratings were  $\sim 75$  nm high, the best fit trapezoidal profiles differed more significantly from the GCT profiles. Figure 8 shows the best fit line profiles for the single trapezoid, double trapezoid, and GCT models. Here the trapezoidal models tended to an almost rectangular shape, and due to reductions in the systematic deviations between data and fit in a few regions of the spectra, actually provided better fits to the ellipsometry data than the GCT model for both the PS18k and PS1570k gratings. However, the SXR profiles and prior work in cross-section SEM imaging of annealed samples<sup>1</sup> suggest that it is unlikely that the gratings would retain such angular profiles after extended annealing, particularly in the low-molecular mass case. This is a somewhat common problem for inverse methods; in some cases, a non-physical model can provide better fits to the data than another model that is better matched to the *a priori* knowledge of the structure. While we are encouraged that the trapezoid models are in agreement with some aspects of the GCT model—for example, the PS1570k again shows a larger line to space ratio than the PS18k grating, which is closer to the 1:1 ratio of a sinusoidal profile—we clearly have difficulty in uniquely determining the profiles from the ellipsometry spectra alone as the grating modulation decreases. The current GCT model has been extremely successful in matching line parameters from AFM and SXR, and in giving line profiles that reasonably match our knowledge of the polymer grating evolution. Subtle differences between gratings of different molecular mass that appear in the late stage annealing GCT profiles, such as degree of corner rounding,<sup>5</sup> need to be further validated through comparison with other profiling methods. However, measurements of line profiles with features measuring in the tens of nanometers are a challenging problem for most techniques, including AFM, SEM and SXR.



**FIG. 8.** Comparison of best fit line profiles obtained using three line profile models for the PS1570k grating at  $\sim 75$  nm height (top, left axis) and for the PS18k grating at  $\sim 75$  nm height (bottom, right axis). The right and left axes have been offset for clarity. The models are the GCT model (light grey solid lines), the single trapezoid model (solid black lines), and the double trapezoid model (dashed red lines).

## 7. SUMMARY AND CONCLUSIONS

In this work, we have demonstrated that scatterometry provides *in situ*, non-destructive measurements of line gratings in nanoimprinted polymers during annealing. In contrast with pattern characterization through *ex situ* methods, scatterometry provides a real-time annealing record from a single sample, and can be used to extract line parameters and shape of the lines at any point during the anneal. The line parameters obtained from the rounded trapezoid (GCT) scatterometry model are in very good agreement with values obtained using AFM and specular x-ray reflectivity (SXR), and preliminary work on comparing the full line profiles of scatterometry and SXR has been presented. Because the choice of line profile model constrains the results of scatterometry analysis, we have also presented line profile results from two simpler, trapezoidal profiles that were applied to a subset of the ellipsometry data. While the trapezoidal profiles agreed fairly well with the GCT profiles early in the annealing and around  $\sim 175$  nm height, deviations between the models were seen for the smallest grating heights investigated. This result reiterates the need for continued refinement of the scatterometry models through comparison of line profile results with other techniques, particularly for gratings with features measured in the tens of nanometers.

## REFERENCES

- [1] Y. Ding, H.W. Ro, K.J. Alvine, B.C. Okerberg, J. Zhou, J.F. Douglas, A. Karim, and C.L. Soles, "Nanoimprint lithography and the role of viscoelasticity in the generation of residual stress in model polystyrene patterns," *Adv. Funct. Mater.* **18**, 1854 (2008).
- [2] Y. Ding, H.W. Ro, T.A. Germer, J.F. Douglas, B.C. Okerberg, A. Karim, and C.L. Soles, "Relaxation behavior of polymer structures fabricated by nanoimprint lithography," *ACSNano* **1**(2), 84 (2007).
- [3] T. Leveder, S. Landis, L. Davoust, S. Soulan, J.-H. Tortai, and N. Chaix, "Surface characterization of imprinted resist above glass transition temperature," *J. Vac. Sci. Technol. B* **25**(6), 2365 (2007).
- [4] R.M. Al-Assaad, L. Tao, and W. Hu, "Physical characterization of nanoimprinted polymer nanostructures using visible light angular scatterometry," *J. Micro/Nanolith. MEMS MOEMS* **7**(1), 013008 (2008).

- 
- [5] H. J. Patrick, T. A. Germer, Y. Ding, H. W. Ro, L. J. Richter, and C. L. Soles, "Scatterometry for *in situ* measurement of pattern reflow in nanoimprinted polymers," *Appl. Phys. Lett.* **93**, 233105 (2008).
- [6] Certain commercial materials and equipment are identified in order to adequately specify the experimental procedure. Such identification does not imply recommendation by the National Institute of Standards and Technology.
- [7] H.G. Tompkins, *A User's Guide to Ellipsometry* (Dover, Mineola, New York, 1993), p. 33.
- [8] C.J. Raymond, "Scatterometry for semiconductor metrology," in *Handbook of Silicon Semiconductor Metrology*, edited by A.C. Diebold (Dekker, New York, 2001), p. 477-514.
- [9] M.G. Moharam, E.B. Grann, D.A. Pommet, and T.K. Gaylord, "Formulation for stable and efficient implementation of the rigorous couple-wave analysis of binary gratings," *J. Opt. Soc. Am. A* **12**(5), 1068-1076 (1995).
- [10] M.G. Moharam, D.A. Pommet, E.B. Grann, and T.K. Gaylord, "Stable implementation of the rigorous coupled-wave analysis for surface-relief gratings: enhanced transmittance matrix approach," *J. Opt. Soc. Am. A* **12**(5), 1077-1086 (1995).
- [11] P. Lalanne and G.M. Morris, "Highly improved convergence of the coupled-wave method for TM polarization," *J. Opt. Soc. Am. A* **13**(4), 779-784 (1996).
- [12] SCATMECH: Polarized Light Scattering Library, available at <http://physics.nist.gov/scatmech>.
- [13] C.M. Herzinger, B. Johs, W.A. McGahan, J.A. Woolam and W. Paulson, "Ellipsometric determination of optical constants for silicon and thermally grown silicon dioxide via a multi-sample, multi-wavelength, multi-angle investigation," *J. Appl. Phys.* **83**(6), 3323-3336 (1998).
- [14] W.H. Press, S.A. Teukolsky, W.T. Vetterling, and B.P. Flannery, *Numerical Recipes in C*, 2<sup>nd</sup> ed., Cambridge, United Kingdom: Cambridge University Press, pp. 689-699, 1992.
- [15] C.M. Herzinger, P.G. Snyder, B. Johs and J.A. Woolam, "InP optical constants between 075 and 5.0 eV determined by variable-angle spectroscopic ellipsometry," *J. Appl. Phys.* **77**(4), 1715 (1995).
- [16] H.J. Patrick and T.A. Germer, "Progress towards traceable nanoscale optical critical dimension metrology in semiconductors," in *Advanced Characterization Techniques for Optics, Semiconductors, and Nanotechnologies III*, A. Duparré, B. Singh, and Z.H. Gu Eds., *Proc. SPIE* **6672**, 66720L-1-9 (2007).
- [17] H.-J. Lee, C.L. Soles, H.W. Ro, R.L. Jones, E.K. Lin, and W. Wu, "Nanoimprint pattern transfer quality from specular x-ray reflectivity," *Appl. Phys. Lett.* **87**, 263111 (2005).
- [18] The slope and intercept uncertainties given here are meant as a rough estimate; they are reported by the program performing the linear regression and are derived by assuming that the scatter in the y-values of the data around the straight line fit is representative of the y uncertainty, then propagating this uncertainty to derive uncertainties in the fit parameters. See for example, P.R. Bevington and D. K. Robinson, *Data Reduction and Error Analysis for the Physical Sciences* 3<sup>rd</sup> ed., McGraw-Hill, New York, pp. 107-110 (2003).
- [19] T.A. Germer, H.J. Patrick, R.M. Silver, and B. Bunday, "Developing an uncertainty analysis for optical scatterometry," in *Metrology, Inspection, and Process Control for Microlithography*, *Proc. SPIE* **7272**, (2009) to be published.